NOTE

Magnetic Resonance in Medicine 00:00–00 (2017)

Anomalous Diffusion in Cerebral Glioma Assessed Using a Fractional Motion Model

Boyan Xu,[1,2] Lu Su,[3] Zhenxiong Wang,[4] Yang Fan,[5] Gaolang Gong,[6] Wenzhen Zhu,[4] Peiyi Gao,[3] and Jia-Hong Gao[1,2,7]*

Purpose: To demonstrate the capability of the fractional motion (FM) model for describing anomalous diffusion in cerebral gliomas and to assess the potential feasibility of FM for grading these tumors.

Methods: Diffusion MRI images were acquired from brain tumor patients using a special Stejskal-Tanner diffusion sequence with variable diffusion gradient amplitudes and separation times. Patients with histopathologically confirmed gliomas, including astrocytic and oligoastrocytic tumors, were selected. The FM-related parameters, including the Noah exponent (α), the Hurst exponent (H), and the memory parameter ($\mu = H - 1/\alpha$), were calculated and compared between low- and high-grade gliomas using a two-sample t-test. The grading performance was evaluated using the receiver operating characteristic analysis.

Results: Twenty-two patients were included in the present study. The calculated α, H, and μ permitted the separation of tumor lesions from surrounding normal tissues in parameter maps and helped differentiate glioma grades. Moreover, α showed greater sensitivity and specificity in distinguishing low- and high-grade gliomas compared with the apparent diffusion coefficient.

Conclusion: The FM model could improve the diagnostic accuracy in differentiating low- and high-grade gliomas. This improved diffusion model may facilitate future studies of neuropathological changes in clinical populations. **Magn Reson Med 000:000–000, 2017. © 2017 International Society for Magnetic Resonance in Medicine.**

Key words: anomalous diffusion; high *b*-value diffusion imaging; cerebral glioma

INTRODUCTION

Diffusion MRI (dMRI) has become a pillar of modern clinical imaging and is being incorporated into general oncologic imaging practice (1,2). Compared with other MRI modalities, dMRI probes the diffusion process in tissues at the cellular scale (e.g., micrometers), well beyond the typical millimetric image resolution (3). The observation of water diffusion in vivo provides unique information about the microscopic properties of biological tissues. Therefore, dMRI has great potential to become a cancer biomarker (2,4). Its clinical applications include characterizing the tumor malignancy, monitoring treatment response, differentiating posttherapeutic changes from residual active tumors and detecting recurrent cancer (2). For example, the most widely used dMRI parameter, the apparent diffusion coefficient (ADC), was found useful in the differentiation of some human brain tumors (5) and tumor grading (6).dMRI is most frequently acquired with b-values ranging from 0 to 1000 s/mm^2 and is quantified using the mono-exponential model, $S/S_0 = \exp(-b \cdot \mathrm{ADC})$, which assumes a normal diffusion process in biological tissues. However, numerous experiments have shown that the observed dMRI signal decay curve deviates from the mono-exponential form in biological tissues, particularly over an extended b-value range (7). To address this problem, several models have been developed to find an optimal agreement between the experimental data and the proposed fitting curves. These models include the bi-exponential model (8,9), the stretched exponential model (10), the statistical model (11), and the kurtosis model (12). In addition to these empirical mathematical models, researchers have also attempted to explain the deviation of signal attenuation through anomalous diffusion processes. Several physics-motivated dMRI models have been proposed based on different theories for various anomalous diffusion processes (13–18). The parameters derived from these models enable a more detailed investigation of differences between tumor types and grades (19–25).

Notably, several studies have indicated that the fractional motion (FM) model is a more appropriate method to describe the diffusion process in living cells (26–30). FM assumes that the diffusion process is α-stable, H-self-similar, and has stationary increments (31). The symbol α denotes the Noah exponent, which quantifies the fluctuations of the random process. The increments are Gaussian distributed when $\alpha = 2$, while the increments are Lévy distributed when $0 < \alpha < 2$. H is the Hurst exponent that describes the self-similarity property of molecular trajectories. The increments of the process are positively correlated and exhibit long-range dependence (long memory, persistence) when the memory parameter is $\mu = H - 1/\alpha > 0$. However, for $\mu<0$, the increments are negatively correlated and exhibit short-range dependence (short memory, antipersistence) (28). In the case of $\mu < 0$, the diffusion process

[1]Beijing City Key Lab for Medical Physics and Engineering, Institute of Heavy Ion Physics, School of Physics, Peking University, Beijing, China.
[2]Center for MRI Research, Academy for Advanced Interdisciplinary Studies, Peking University, Beijing, China.
[3]Department of Radiology, Beijing Tiantan Hospital, Capital Medical University, Beijing, China.
[4]Department of Radiology, Tongji Hospital, Tongji Medical College, Huazhong University of Science and Technology, Wuhan, China.
[5]MR Research China, GE Healthcare, Beijing, China.
[6]State Key Laboratory of Cognitive Neuroscience and Learning, Beijing Normal University, Beijing, China.
[7]McGovern Institute for Brain Research, Peking University, Beijing, China

Grant sponsor: National Natural Science Foundation of China; Grant numbers: 31421003, 81227003, 81430037; Grant sponsor: Beijing Municipal Science & Technology Commission; Grant number: Z161100000216152.

*Correspondence to: Jia-Hong Gao, Ph.D., Center for MRI Research, Peking University, Beijing, China 100871. E-mail: jgao@pku.edu.cn

Received 23 June 2016; revised 22 October 2016; accepted 22 November 2016
DOI 10.1002/mrm.26581
Published online 00 Month 2017 in Wiley Online Library (wileyonlinelibrary.com).

follows a subdiffusive pattern (28), which has been observed in living cells (32).

The FM-based dMRI theory has only recently been proposed, and the spatially resolved FM-related parameter maps of healthy volunteers have been obtained, showing remarkable contrasts among normal brain tissues (18). However, the FM model has not yet been applied to any brain diseases. The assessment of the relationship between the parameters (α, H and μ) of the FM model and tumor histopathology would enable the detection of differences among tumor types and grades with high sensitivity. In this note, the FM model was investigated in cerebral gliomas, the most common type of primary brain tumor. The purpose of the present study was to evaluate the potential value of the FM model in differentiating grades of gliomas.

METHODS

Patients

This study was approved by the local institutional review board and was performed in compliance with the Health Insurance Portability and Accountability Act. Informed consent was obtained from all participants. A total of 50 adult patients with brain tumors underwent MRI examination. Patients were selected if they met the following criteria: (a) MR imaging was performed before the treatment of tumors; (b) patient had no concurrent brain diseases unrelated to the tumor; and (c) a histopathological diagnosis of glioma was assigned after surgical resection.

Image Acquisition

MR imaging was performed on a 3 Tesla (T) GE Discovery MR750 MRI scanner (GE Healthcare, Milwaukee, Wisconsin) equipped with an eight-channel head coil. All dMRI images were obtained using a special Stejskal-Tanner single-shot spin-echo echo-planar-imaging sequence. To fit the FM model, the diffusion gradient separation time (Δ) was not fixed during the scanning process as the conventional dMRI sequence. Specifically, Δ was arrayed at 27.5, 40.0, and 55.5 ms. For each Δ value, the diffusion gradient amplitude (G_0) was arrayed at 15.67, 19.68, 24.73, 31.06, 39.01, and 49.00 mT/m, which were chosen to be approximately evenly spaced on a log axis. The gradient duration constant (δ) was kept constant (20.4 ms). Therefore, a total of 18 nonzero b-values were produced in each gradient direction (151, 239, 377, 595, 938, 1480, 243, 383, 604, 954, 1504, 2374, 356, 562, 887, 1399, 2207, and 3482 s/mm^2). The diffusion gradients were successively applied in three orthogonal directions (the x-axis, y-axis, and z-axis) to minimize the effect of diffusion anisotropy. In addition, a total of 12 images without diffusion sensitization ($b = 0$) were obtained. The other data acquisition parameters for this diffusion sequence were: TR/TE = 3800 ms/110 ms; accelerating factor = 2; field-of-view = 24 cm × 24 cm; matrix size = 128 × 128; slice thickness = 5 mm; and number of excitations = 2. The total scan time was 8 min and 42 s to facilitate clinical use. In addition, routine MRI examinations were performed, including gadolinium contrast-enhanced T_1-weighted imaging and T_2-weighted imaging.

Image Analysis

Before image analysis, the acquired images were corrected for eddy current distortions and head motions using FSL tools (33). ADC maps were calculated using the images acquired at b-values of 0 and 954 s/mm^2. To obtain the anomalous diffusion parameters, the images were analyzed using the FM model. According to the FM-based dMRI theory (18), the diffusion induced signal decay can be formulated as

$$S/S_0 = \exp(-D_{\alpha,H} b_{\alpha,H}) \quad [1]$$

where $D_{\alpha,H}$ is the generalized diffusion coefficient of anomalous diffusion, and $b_{\alpha,H}$ is the generalized b-value. When using the Stejskal-Tanner diffusion sequence (34), this generalized b-value can be calculated as

$$b_{\alpha,H} = \eta \cdot \gamma^{\alpha} G_0^{\alpha} \Delta^{\alpha+\alpha H} \quad [2]$$

where γ is the gyromagnetic ratio. As mentioned above, G_0 is the diffusion gradient amplitude, and Δ is the gradient separation time. In Equation [2], η is a dimensionless number, which can be calculated using the formula

$$\eta = \frac{1}{(1+\mu)^{\alpha}}\left[\int_0^{\delta/\Delta}\left|\left(\frac{\delta}{\Delta}+1-u\right)^{1+\mu} - (1-u)^{1+\mu} - \left(\frac{\delta}{\Delta}-u\right)^{1+\mu}\right|^{\alpha} du + \int_{\delta/\Delta}^{1}\left|\left(\frac{\delta}{\Delta}+1-u\right)^{1+\mu} - (1-u)^{1+\mu}\right|^{\alpha} du + \int_1^{1+\delta/\Delta}\left(\frac{\delta}{\Delta}+1-u\right)^{\alpha+\alpha\mu} du\right] \quad [3]$$

The signal attenuation at each voxel was fitted to Equation [1] separately along each direction. Directionally averaged maps were subsequently calculated to reduce the influence of anisotropy. All fitting procedures were performed using the trust-region-reflective nonlinear fitting algorithm in Matlab (MathWorks, Natick, MA).

Two radiologists (Z.W., L.S.) who were in consensus manually drew the region of interest (ROI) for tumor and normal-appearing white matter (NAWM) on the T_2-weighed echo-planar images (i.e., the dMRI images with b-values of 0 s/mm^2) according to the contrast-enhanced T_1-weighted images and T_2-weighted images. The selected tumor ROIs included only the solid region of the tumor, despite enhancement. The NAWM ROI was drawn in contralateral normal-appearing centrum semiovale to the tumor ROI, with the same size. In all cases, the ROI size and placement were selected to exclude ambiguous voxels and avoid partial volume effects. When selecting the ROIs, the two radiologists were blinded to all parameter maps. Subsequently, the mean values of the estimated ADC, α, H, and μ were calculated

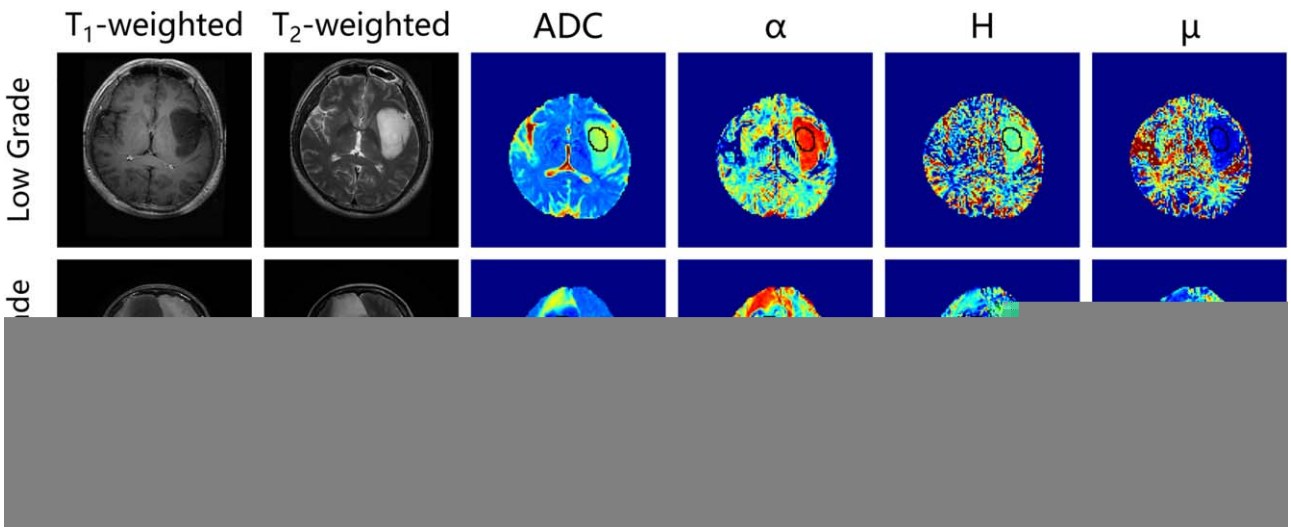

FIG. 1. Representative axial MR images and parameter maps from one low-grade patient [top row, a 36-year-old male with astrocytoma (WHO grade II)], and one high-grade patient [bottom row, a 38-year-old female with glioblastoma (WHO grade IV)]. The solid tumor ROIs are shown with black contours in the parameter maps.

over the selected ROIs. To objectively quantify tumor conspicuity, the relative parameters (ADC_r, α_r, H_r, and μ_r) were generated by dividing the mean value in tumor ROI by the mean value in the corresponding NAWM.

To assess the feasibility of the FM model for tumor grading, the mean values for ADC, α, H, and μ of the tumor ROIs and the relative parameters to the contralateral NAWM were compared among high- and low-grade gliomas using a two-sample t-test. A probability of less than 5% (P-values < 0.05) was considered statistically significant. Moreover, to quantify the overall sensitivity and specificity of these parameters in differentiating low- and high-grade gliomas, receiver operating characteristic (ROC) curves were generated to assess the area under the curve (AUC).

RESULTS

Overall, 22 patients were included in the present study (15 males and 7 females; mean age, 43.0 years; age range, 25–60 years). According to the World Health Organization (WHO) criteria (35), this patient group comprised 16 astrocytic tumors (4 WHO grade II, 1 WHO grade III, and 11 WHO grade IV) and 6 oligoastrocytic tumors (2 WHO grade II and 4 WHO grade III). The patients were divided into low-grade (WHO grade I or II; n = 6; 1 female; mean age, 40.5 years; age range, 31–60 years) and high-grade (WHO grade III or IV; n = 16; 6 females; mean age, 43.9 years; age range, 25–59 years) tumor groups.

To evaluate the fitting procedures in the tumor regions, the mean values of the fitting residuals over both tumor and contralateral NAWM ROIs were calculated. The results of the paired t-test showed that the mean fitting residuals of tumor ROIs were significantly lower than those of the contralateral NAWM ROIs (P-values < 0.001) indicating that the FM-model matches the tumor data well.

Representative imaging results for this patient group are shown in Figure 1. The directionally averaged maps of the FM-related parameters (α, H, and μ), contrast-enhanced T_1-weighted images, the T_2-weighted images and the directionally averaged ADC maps are shown. On the α, H, and μ maps, the contrast of normal gray matter/white matter/cerebrospinal fluid in the FM-related parameter maps was similar to the contrast depicted in a previous study involving healthy subjects (18). On the other hand, the α, H, and μ maps showed a clear distinction of tumor lesions and peritumoral edemas from normal tissues.

The mean values of the parameters in both tumor and NAWM ROIs are summarized in Table 1. Figure 2 displays scatter diagrams of α versus H and μ. Together with the mean values for all tumor ROIs, the relative parameters were also plotted to eliminate the individual difference effect. As Figure 2 depicts, the brain tumor and NAWM can be readily separated using α, H, and μ, even when these parameters of tumor ROIs widely varied. Moreover, Figure 2 demonstrates the separation between high- and low-grade gliomas based on FM-related parameters. Significant differences were observed between high- and low-gliomas for the mean α (P-value < 0.0001), μ (P-value < 0.01), and ADC (P-value < 0.05), whereas H (P-value $= 0.48$) failed to differentiate between high- and low-grade gliomas. The same results were obtained using the relative parameters, where α, μ, and ADC succeeded in differentiating high- and low-grade gliomas (P-value < 0.001 for α, P-value < 0.05 for μ, and P-value < 0.05 for ADC), but H failed to differentiate these tumors (P-value $= 0.40$).

The performance in differentiating low-grade and high-grade gliomas was also illustrated in the ROC analysis. Figures 3a,b display the ROC curves calculated from the mean and relative values, respectively, for all tumors. Although influenced by the limited number of cases, larger AUCs were obtained with α (AUC = 0.98 in Figure 3a, AUC = 0.96 in Figure 3b) and μ (AUC = 0.99 in Figure 3a, AUC = 0.84 in Figure 3b) compared with ADC (AUC = 0.83 in Figure 3a, AUC = 0.88 in Figure 3b); H exhibited the smallest AUC (AUC = 0.59 in Figure 3a,

Table 1
Mean and SD of the FM-Related Parameters and ADC for Tumor and Normal-Appearing White Matter (NAWM) Regions

		FM-related parameters		
Tissue	ADC ($\times 10^{-3}$ mm^2/s)	α	H	μ
NAWM	0.73 ± 0.04	1.45 ± 0.05	0.43 ± 0.05	-0.26 ± 0.07
Low-grade glioma	1.5 ± 0.2	1.84 ± 0.06	0.49 ± 0.02	-0.05 ± 0.02
High-grade glioma	1.1 ± 0.3	1.6 ± 0.1	0.48 ± 0.06	-0.15 ± 0.08

AUC = 0.64 in Figure 3b). For α, the highest Youden index (sum of sensitivity and specificity minus one) was reached when $1.70 \leq \alpha \leq 1.73$, while the optimal threshold for μ was between -0.077 and -0.073. Moreover, α_r in range from 1.16 to 1.19 maximized the Youden index. These findings suggest the potential feasibility of FM-related parameters, particularly α, in distinguishing between low- and high-grade gliomas.

DISCUSSION

In the present study, the FM model was applied to analyze anomalous diffusion in tumor lesions in vivo. The FM-related parameters exhibited remarkable image contrasts that related to the anomalous diffusion, which were different from ADC. Although it is difficult to fully clarify the relationship between FM-related parameters and tumor characteristics from the limited number of patients included in the present study, these parameters were useful for differentiating low- and high-grade gliomas. Notably, α provides a higher sensitivity and specificity than the most commonly used diffusion parameter, ADC, for grading gliomas. Additional studies using a large population would increase the statistical power for sounder conclusions.

The FM-related parameter values in gliomas, particularly high-grade gliomas, varied over a large range. In addition to the differences in types and grades, this phenomenon can result from several causes. High-grade tumors are histologically heterogeneous (36,37), influenced by tumor cellularity, nuclear atypia, pleomorphism, and nuclear-to-cytoplasmic ratio. Other components may also contribute to this phenomenon, including necroses, cysts, and tortuous vascular hyperplasia within tumor matrix (36,38,39). Taken together, these factors diversify the microstructure of histologic tissue and lead to variations in FM-related parameters.

As shown in Equation [2], α is an exponent of the diffusion gradient that is mathematically proportional to

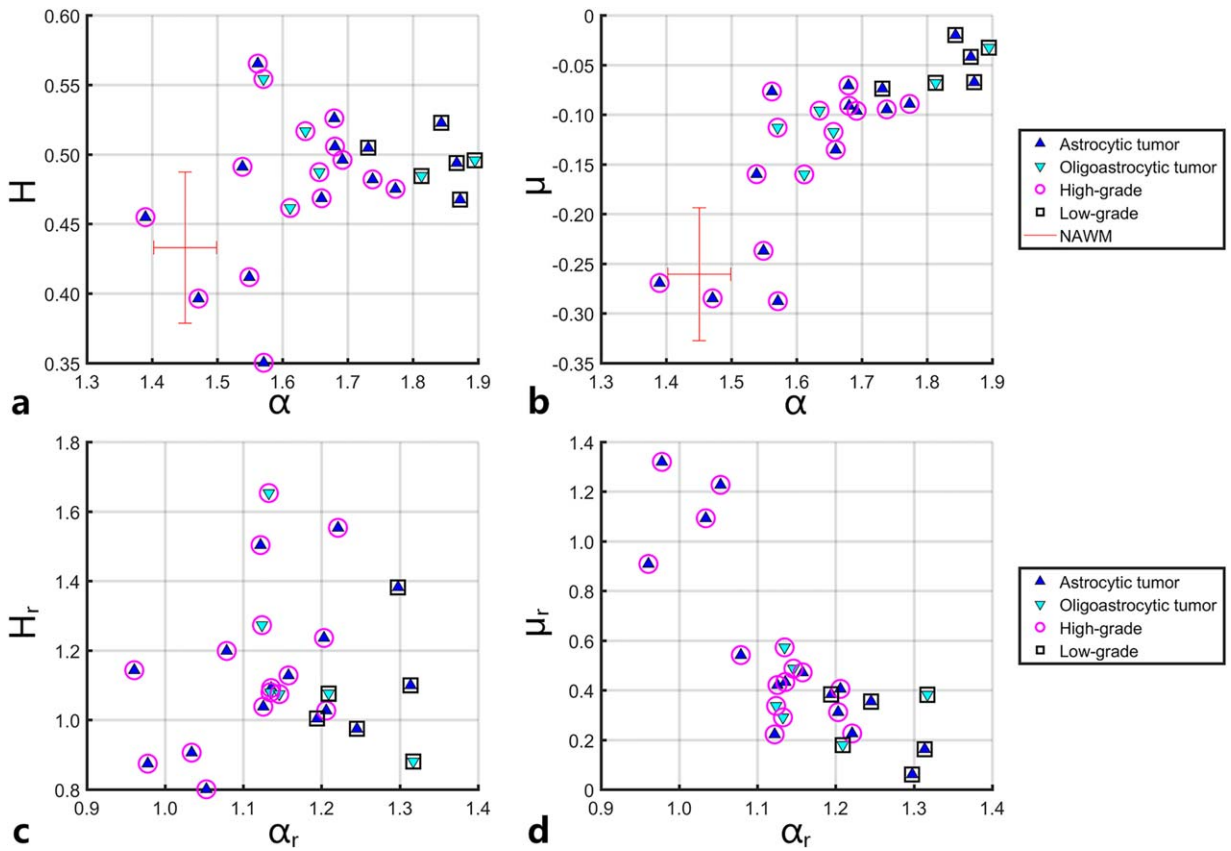

FIG. 2. Scatter diagrams of α versus *H* and μ. Both the mean values for all tumor ROIs (**a,b**) and the relative parameters to contralateral normal-appearing white matter (NAWM) (**c,d**) are plotted. All gliomas are classified according to type and grade. The parameter values for the NAWM regions are displayed for reference.

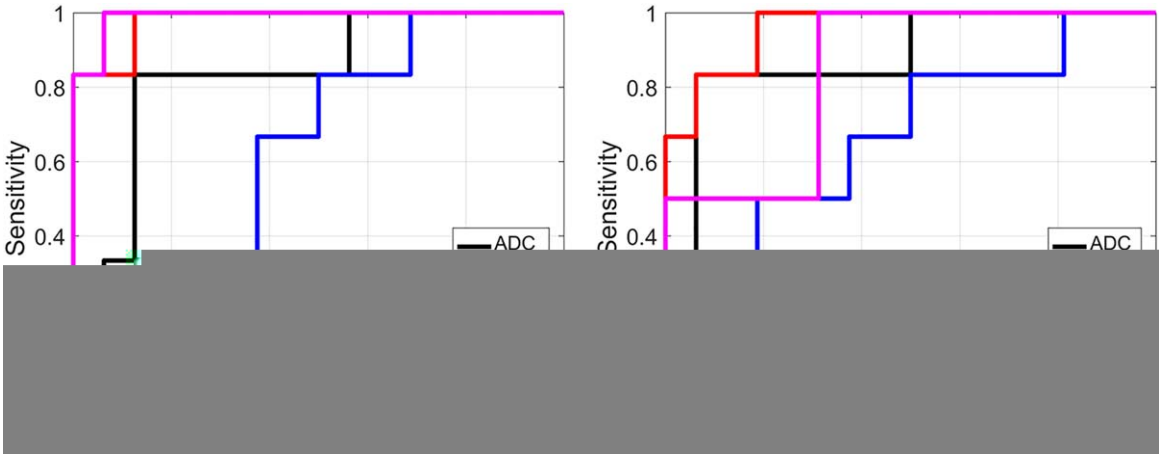

FIG. 3. Receiver operating characteristic (ROC) curves obtained using ADC, α, *H*, and μ for differentiating low- and high-grade gliomas. The ROC curves were generated using the mean values for all tumors (**a**) and the relative values to contralateral normal-appearing white matter (**b**).

the parameters proposed by other dMRI models, such as the stretching parameter in the stretched-exponential model (10,16,40). These parameters are consistent with the α in gray matter, white matter, and cerebrospinal fluid, indicating that the calculation of FM-related parameters is reliable. While these parameters have been explained as an index of heterogeneity in water diffusion, α describes the variances of increments of diffusion processes according to the FM theory (18,31). To fully clarify the relationship between the imaging parameters and pathological changes, the precise diffusion process in tumor tissue should be further explored.

The limitations of the present study must be acknowledged. First, the use of single-shot echo-planar imaging may lead to image distortion and signal loss. Although these artifacts have been considerably reduced as a result of the development of high-performance gradients and parallel imaging, they may still occur, and the evaluation of the tumors in these areas may be confined. Second, the voxel was large, and a single voxel depicted an aggregated measure of the neuronal environment for a large sample size, which may hamper sensitivity to tissue components occupying a small fraction of a voxel. Another limitation is the sampling bias of the ROIs as a result of tissue heterogeneity. The direct voxel-wise radiologic-pathologic correlation should be further explored.

Notably, diffusion in brain tissue is known to be directionally dependent, that is, anisotropic. Diffusion tensor imaging is the most commonly used approach to describe diffusion anisotropy in tissue. With maps showing anisotropy, tumor growth-related changes in white matter, such as tumor infiltration or invasion, can be observed (41). Moreover, advanced models that characterize diffusion anisotropy could improve the delineation of tumors from NAWM (42). With anisotropy considered, the FM model may offer improved clinical utility. A study of the anisotropy of the parameter maps of the FM model is currently under way.

CONCLUSIONS

In summary, the FM model was successfully applied in cerebral glioma cases, and the results indicated that the anomalous diffusion parameter images could assist in grading gliomas. The utility of this model may lead to a new perspective on investigating pathological changes in tissues.

ACKNOWLEDGMENTS

B.X., L.S., and Z.W. contributed equally to this work.

REFERENCES

1. Iima M, Le Bihan D. Clinical intravoxel incoherent motion and diffusion MR imaging: past, present, and future. Radiology 2015;278:13–32.
2. Padhani AR, Liu G, Mu-Koh D, et al. Diffusion-weighted magnetic resonance imaging as a cancer biomarker: consensus and recommendations. Neoplasia 2009;11:102–125.
3. Le Bihan D, Johansen-Berg H. Diffusion MRI at 25: Exploring brain tissue structure and function. Neuroimage 2012;61:324–341.
4. Patterson DM, Padhani AR, Collins DJ. Technology insight: water diffusion MRI—a potential new biomarker of response to cancer therapy. Nat Clin Pract Oncol 2008;5:220–233.
5. Yamasaki F, Kurisu K, Satoh K, et al. Apparent diffusion coefficient of human brain tumors at MR imaging. Radiology 2005;235:985–991.
6. Bulakbasi N, Guvenc I, Onguru O, Erdogan E, Tayfun C, Ucoz T. The added value of the apparent diffusion coefficient calculation to magnetic resonance imaging in the differentiation and grading of malignant brain tumors. J Comput Assist Tomogr 2004;28:735–746.
7. De Santis S, Gabrielli A, Palombo M, Maraviglia B, Capuani S. Non-Gaussian diffusion imaging: a brief practical review. Magn Reson Imaging 2011;29:1410–1416.
8. Niendorf T, Dijkhuizen RM, Norris DG, van Lookeren Campagne M, Nicolay K. Biexponential diffusion attenuation in various states of brain tissue: implications for diffusion-weighted imaging. Magn Reson Med 1996;36:847–857.
9. Mulkern RV, Gudbjartsson H, Westin C-F, et al. Multi-component apparent diffusion coefficients in human brain. NMR Biomed 1999; 12:51–62.
10. Bennett KM, Schmainda KM, Bennett (Tong) R, Rowe DB, Lu H, Hyde JS. Characterization of continuously distributed cortical water diffusion rates with a stretched-exponential model. Magn Reson Med 2003;50:727–734.
11. Yablonskiy DA, Bretthorst GL, Ackerman JJH. Statistical model for diffusion attenuated MR signal. Magn Reson Med 2003;50:664–669.
12. Jensen JH, Helpern JA, Ramani A, Lu H, Kaczynski K. Diffusional Kurtosis imaging: the quantification of non-gaussian water diffusion by means of magnetic resonance imaging. Magn Reson Med 2005;53: 1432–1440.
13. Özarslan E, Basser PJ, Shepherd TM, Thelwall PE, Vemuri BC, Blackband SJ. Observation of anomalous diffusion in excised tissue by characterizing the diffusion-time dependence of the MR signal. J Magn Reson 2006;183:315–323.

14. Magin RL, Abdullah O, Baleanu D, Zhou XJ. Anomalous diffusion expressed through fractional order differential operators in the Bloch–Torrey equation. J Magn Reson 2008;190:255–270.
15. Cooke JM, Kalmykov YP, Coffey WT, Kerskens CM. Langevin equation approach to diffusion magnetic resonance imaging. Phys Rev E 2009;80:61102.
16. Zhou XJ, Gao Q, Abdullah O, Magin RL. Studies of anomalous diffusion in the human brain using fractional order calculus. Magn Reson Med 2010;63:562–569.
17. Ingo C, Magin RL, Colon-Perez L, Triplett W, Mareci TH. On random walks and entropy in diffusion-weighted magnetic resonance imaging studies of neural tissue. Magn Reson Med 2014;71:617–627.
18. Fan Y, Gao J-H. Fractional motion model for characterization of anomalous diffusion from NMR signals. Phys Rev E 2015;92:12707.
19. Maier SE, Bogner P, Bajzik G, Mamata H, Mamata Y, Repa I, Jolesz FA, Mulkern RV. Normal brain and brain tumor: multicomponent apparent diffusion coefficient line scan imaging. Radiology 2001;219: 842–849.
20. Mardor Y, Pfeffer R, Spiegelmann R, et al. Early detection of response to radiation therapy in patients with brain malignancies using conventional and high B-value diffusion-weighted magnetic resonance imaging. J Clin Oncol 2003;21:1094–1100.
21. Kwee TC, Galbán CJ, Tsien C, et al. Intravoxel water diffusion heterogeneity imaging of human high-grade gliomas. NMR Biomed 2010;23: 179–187.
22. Kwee TC, Galbán CJ, Tsien C, et al. Comparison of apparent diffusion coefficients and distributed diffusion coefficients in high-grade gliomas. J Magn Reson Imaging 2010;31:531–537.
23. Van Cauter S, Veraart J, Sijbers J, et al. Gliomas: diffusion kurtosis MR imaging in grading. Radiology 2012;263:492–501.
24. Sui Y, Wang H, Liu G, Damen FW, Wanamaker C, Li Y, Zhou XJ. Differentiation of low- and high-grade pediatric brain tumors with high B-value diffusion-weighted MR imaging and a fractional order calculus model. Radiology 2015:142156.
25. Karaman MM, Sui Y, Wang H, Magin RL, Li Y, Zhou XJ. Differentiating low- and high-grade pediatric brain tumors using a continuous-time random-walk diffusion model at high B-values. Magn Reson Med 2016;76:1149–1157.
26. Magdziarz M, Weron A, Burnecki K, Klafter J. Fractional Brownian motion versus the continuous-time random walk: a simple test for subdiffusive dynamics. Phys Rev Lett 2009;103:180602.
27. Szymanski J, Weiss M. Elucidating the origin of anomalous diffusion in crowded fluids. Phys Rev Lett 2009;103:38102.
28. Burnecki K, Weron A. Fractional L'evy stable motion can model subdiffusive dynamics. Phys Rev E 2010;82:21130.
29. Ernst D, Hellmann M, Köhler J, Weiss M. Fractional Brownian motion in crowded fluids. Soft Matter 2012;8:4886–4889.
30. Weiss M. Single-particle tracking data reveal anticorrelated fractional Brownian motion in crowded fluids. Phys Rev E 2013;88:10101.
31. Eliazar II, Shlesinger MF. Fractional motions. Phys Rep 2013;527: 101–129.
32. Golding I, Cox EC. Physical nature of bacterial cytoplasm. Phys Rev Lett 2006;96:98102.
33. Smith SM, Jenkinson M, Woolrich MW, et al. Advances in functional and structural MR image analysis and implementation as FSL. Neuroimage 2004;23(Suppl 1):S208–S219.
34. Stejskal E, Tanner J. Spin diffusion measurements: spin echoes in the presence of a time-dependent field gradient. J Chem Phys 1965;42: 288–300.
35. Louis DN, Ohgaki H, Wiestler OD, Cavenee WK, Burger PC, Jouvet A, Scheithauer BW, Kleihues P. The 2007 WHO classification of tumours of the central nervous system. Acta Neuropathol (Berl) 2007; 114:97–109.
36. Marusyk A, Polyak K. Tumor heterogeneity: causes and consequences. Biochim Biophys Acta 2010;1805:105–117.
37. Sottoriva A, Spiteri I, Piccirillo SGM, Touloumis A, Collins VP, Marioni JC, Curtis C, Watts C, Tavaré S. Intratumor heterogeneity in human glioblastoma reflects cancer evolutionary dynamics. Proc Natl Acad Sci U S A 2013;110:4009–4014.
38. Cha S. Update on brain tumor imaging: from anatomy to physiology. AJNR Am J Neuroradiol 2006;27:475–487.
39. Ricard D, Idbaih A, Ducray F, Lahutte M, Hoang-Xuan K, Delattre J-Y. Primary brain tumours in adults. Lancet 2012;379:1984–1996.
40. Hall MG, Barrick TR. From diffusion-weighted MRI to anomalous diffusion imaging. Magn Reson Med 2008;59:447–455.
41. Maier SE, Sun Y, Mulkern RV. Diffusion Imaging of Brain Tumors. NMR Biomed 2010;23:849–864.
42. White NS, McDonald CR, Farid N, Kuperman JM, Kesari S, Dale AM. Improved conspicuity and delineation of high-grade primary and metastatic brain tumors using "restriction spectrum imaging": quantitative comparison with high B-value DWI and ADC. AJNR Am J Neuroradiol 2013;34:958–964.